HHS Public Access

Author manuscript

Acc Chem Res. Author manuscript; available in PMC 2020 June 19.

Published in final edited form as:

Acc Chem Res. 2018 November 20; 51(11): 2897–2905. doi:10.1021/acs.accounts.8b00351.

Acoustogenic Probes: A New Frontier in Photoacoustic Imaging

Hailey J. Knox, **Jefferson Chan***

Department of Chemistry and Beckman Institute for Advanced Science and Technology, University of Illinois at Urbana-Champaign, 600 S. Mathews Ave., Urbana, IL, 61801

CONSPECTUS

Photoacoustic imaging (PAI) is a powerful imaging modality capable of mapping the absorption of light in biological tissue via the PA effect. When chromophores are optically excited, subsequent energy loss in the form of heat generates local thermoelastic expansion. Repeated excitation from a pulsed laser induces pressure fluctuations that propagate through tissue and can be detected as ultrasound waves. By combining ultrasonic detection with optical excitation, PAI enables high-resolution image acquisition at centimeter depths. PAI is also relatively inexpensive and relies on safe, non-ionizing excitation light in the near-infrared window, making it an attractive alternative to other common biomedical imaging modalities.

Research in our group is aimed at developing small-molecule activatable probes that can be used for analyte detection in deep tissue via PAI. These probes contain reactive triggers that undergo a selective chemical reaction in the presence of specific stimuli to produce a spectral change, that can be observed via PAI. Chemically tuning the absorbance profile of the probe and the reacted product such that they are both within the PA imaging window enables ratiometric imaging when each species is irradiated at a specific wavelength. Ratiometric imaging is an important design feature of these probes as it minimizes error associated with tissue-dependent signal fluctuations and instrumental variation.

In this account, we discuss key properties for designing small-molecule PA probes that can be applied for *in vivo* studies and the challenges associated with this area of probe development. We also highlight examples from our group including probes capable of detecting metal ions (Cu(II)), reactive nitrogen species (NO), and oxygen tension (hypoxia). Each of these targets can be sensed using a modular design strategy based on influencing the electronic and spectral properties of a NIR-absorbing dye platform. We demonstrate that ideal PA probes have high molar absorptivity, low fluorescence quantum yields, and selective triggers that can reliably report on a single analyte in a complex biological setting. Probes must also be highly chemo- and photostable to enable long term imaging studies. We show that these PA probes react rapidly and selectively and can be utilized for deep-tissue imaging in mouse models of various diseases. Overall, these examples represent a new class of biomedical imaging tools that seek to enable high resolution molecular imaging capable of improving diagnostic methods and elucidating new biological discoveries. We anticipate that the combination of small-molecule PA probes with new PAI technology will enable

***Corresponding Author**: Tel.: 217-300-2767 jeffchan@illinois.edu.

The authors declare no competing financial interest.

non-invasive detection of analytes relevant to disease progression and mapping of tissue microenvironments.

Conspectus Graphic

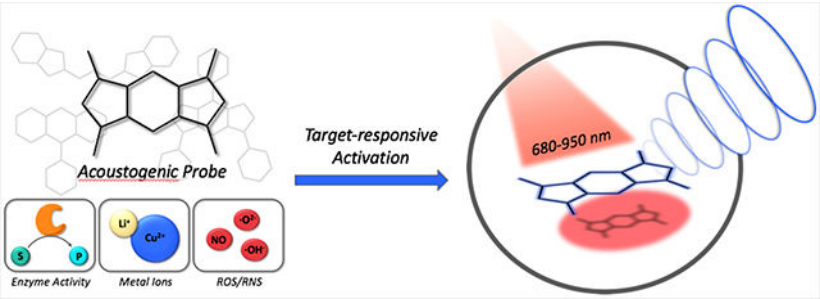

INTRODUCTION

The complexity of living systems has presented scientists with the immense challenge of understanding biological phenomena in their native contexts. Molecular imaging has enabled visualization of dynamic events occurring at the cellular and molecular levels in intact samples and living organisms. The observation of an array of chemical reactions and signaling networks that contribute to both physiology and pathology has led to fundamental and translational scientific advances including improved diagnostics and real-time therapy monitoring.

Molecular imaging refers to the use of specialized instrumentation with or without targeted imaging agents to non-invasively observe biochemical processes and tissue characteristics in real time.[1] Historically, imaging agents used for molecular imaging consist of a targeting unit appended to a signal-emitting component (e.g., radionuclide), and target detection relies on accumulation-based signal enhancement. An alternative approach aimed at improving sensitivity involves activatable probes in which the signal is “off” until the probe undergoes a target-specific chemical reaction to provide a turn-on response.[2] Fluorogenic probes are the most common members in this family and have been employed in an impressive array of live-cell imaging applications.[3] However, the utility of these imaging agents *in vivo* is limited to shallow imaging depths (< 1 mm) due to tissue-induced light scattering.[4]

Our goal is to combine photoacoustic imaging (PAI) with activatable probes that can be used in deep tissue for both diagnostic and basic scientific applications. PAI relies on optical excitation of a chromophore, followed by vibrational relaxation to release energy as heat.[5] This induces a local temperature increase and thermoelastic expansion, propagating pressure waves that are detected using ultrasound transducers and digitalized to produce a 3D image. The combination of optical excitation with ultrasonic detection results in high-resolution image acquisition at centimeter depths. PAI utilizes near-infrared (NIR) light that can penetrate deep into tissue and minimize light-induced damage. The utility of PAI for detecting endogenous chromophores (e.g., hemoglobin) has already been demonstrated for numerous clinical applications.[6] In this Account, we describe general design considerations

for small-molecule PA probes and our application of these strategies to develop activatable probes for analytes and microenvironments implicated in disease pathology.

PA PROBE DESIGN PRINCIPLES

When designing PA probes, it is essential to consider three key photophysical properties of the chromophore. First, the wavelength of maximum absorbance (λ_{abs}) should fall between 680 and 950 nm because interference from tissue absorbance is minimized and commercial PA tomographers rely on a tunable laser operating within this wavelength range. Second, the fluorescence quantum yield should be low to maximize the energy dissipated through non-radiative pathways, resulting in a greater PA signal.[7] Finally, the chromophore should exhibit a large extinction coefficient ($>10^4$ $M^{-1}cm^{-1}$) to maximize the amount of incident light absorbed.

NIR fluorescent dyes and quenchers featuring characteristics mentioned above have been repurposed to provide exogenous PA contrast in several studies.[8,9] In 2010, Gambhir and coworkers demonstrated the first activatable PA probe with a design that relies on enzymatic cleavage of two NIR chromophores linked by a peptide backbone.[10] While this approach was effective for imaging endoprotease activity, we sought to establish a more general design based on a single small-molecule chromophore that could be tuned to respond to a specific stimulus.[11]

Our early designs involved modulating the quantum yield as a function of probe turnover. We rationalized that if a probe was highly fluorescent, it would exhibit a low PA signal output since radiative and non-radiative processes are competing pathways.[7] This PA signal could then be enhanced to give a turn-on response if fluorescence became quenched upon probe activation. However, many other parameters also contribute to the strength of the PA signal, including solubility, triplet state contributions, excited state absorption, relaxation kinetics, and photobleaching.[12,13] Thus, we found that the quantum yield alone is not a reliable predictor of PA signal. We then turned our attention to a design in which activation would result in a shift in the molecule's absorbance to produce a spectrally distinct product (Figure 1). This enables detection of a PA turn-on response at a wavelength where previously little to no signal could be detected, and it allows for ratiometric imaging if both states of the probe produce signal within the desired wavelength range. Ratiometric imaging is a key highlight of this strategy as it accounts for factors commonly known to cause signal variation such as local probe concentration, tissue-dependent signal attenuation, and fluctuations in the irradiation source intensity.[14] In our studies, ratiometric fold turn-on is defined as the fold enhancement of a ratiometric PA signal upon probe activation (Eq. 1).

$$\frac{PA(\lambda_2)_{final} \,/\, PA(\lambda_1)_{final}}{PA(\lambda_2)_{inital} \,/\, (\lambda_1)_{inital}} \qquad \text{Equation 1:}$$

Work published in 2012 by Klimant demonstrated that the absorbance maximum for an aza-BODIPY dye could be tuned based on its protonation state.[15] This study reports a large pH-dependent shift in the absorbance maximum (~90 nm) when an aza-BODIPY-based probe containing an *o*-chloro phenol is deprotonated. Other studies have shown that this trend is

consistent for aza-BODIPY dyes; increasing electron donation into the conjugated system provides a bathochromic (red) shift in the absorbance, while a hypsochromic (blue) shift results when electron density is removed with electron-withdrawing substituents.[16] This inspired our general strategy in which manipulation of the electronics of the aza-BODIPY dye platform produces a spectral change that can be detected using PAI. We have termed these small-molecule probes “acoustogenic” to indicate a selective PA turn-on response to a particular analyte of interest.[11,17]

METAL ION-RESPONSIVE PROBES

Misregulation of Cu(II) is known to play a role in cancer and neurodegenerative diseases including Alzheimer’s disease and amyotrophic lateral sclerosis.[18] Developing tools capable of detecting Cu(II) in deep tissue can help to further our understanding of its roles in disease progression. This motivated our development of Acoustogenic Probes for Copper(II) (APC).[17] APC-1 and APC-2 (a water-soluble congener) each consist of a Cu(II)-responsive picolinic ester appended to an aza-BODIPY dye. Coordination of Cu(II) activates the ester for hydrolysis, resulting in uncapping of a phenoxide product (Figure 2a). Similar to Klimant’s work,[15] we relied on installation of ortho substituents to modulate the phenol pK_a. The dichloro structure resulted in a lower phenol pK_a of ~4.5, ensuring that the product is fully deprotonated in a biological setting. As predicted, the conversion of an electron-withdrawing ester to an electron-donating phenoxide produces a 70 nm red shift in the probe absorbance (Figure 2b). Ratiometric imaging can therefore be used to detect Cu(II) by determining the PA signals produced at 697 and 767 nm, corresponding to the parent probe and its hydrolyzed product, respectively (Figure 2e). The addition of just one equivalent of Cu(II) to a solution of APC-2 elicited a 91.3-fold ratiometric PA turn-on response, while 10 equivalents produced a 100.5-fold turn-on response (Figure 2c). Selectivity studies and metal ion competition experiments revealed that probe activation was selective for Cu(II) (Figure 2d).

PA evaluation of APC-2 was carried out by acquiring images of probe solutions in fluorinated ethylene propylene (FEP) tubing placed inside an agarose-based tissue-mimicking phantom (Figure 2e). Of note, this method has become standard practice in our group for *in vitro* evaluation of probe PA signal. To demonstrate that PA signal from APC-2 could still be detected in the presence of endogenous absorbers like proteins and lipids, images were also acquired of APC-2 in chicken breast tissue cut to the same dimensions as our tissue-mimicking phantoms. These results indicated that the PA signal of the aza-BODIPY dye would be sufficient for imaging in biological tissue.

APC-1 and -2 show that a single chromophore can be used for analyte-responsive PAI if it is designed to undergo a spectral change upon activation. This work paved the way for further applications of this wavelength-shift approach and indicated that the aza-BODIPY platform could serve as a generalizable PA chromophore for a variety of applications. Ongoing work in our group is aimed at expanding the toolbox of acoustogenic probes for sensing other metal ions and applying these probes *in vivo*. A major challenge is to develop probes with the sensitivity to detect the metal ion of interest under physiologically relevant concentrations. A complementary approach to our strategy was demonstrated by Westmeyer

in which PA imaging of calcium could be achieved by a probe that undergoes reversible ion chelation.[19]

NITRIC OXIDE-RESPONSIVE PROBES

Non-invasive detection of nitric oxide (NO) is of interest due to its many roles in biological signaling pathways, but presents a challenge due to the limited resolution and sensitivity of established methods.[20,21] We hypothesized that PAI with an NO-responsive acoustogenic probe could address these challenges and enable new investigations such as longitudinal tracking of NO production during disease progression.

An important consideration in acoustogenic NO probe design is the selection of a responsive trigger. Most reported NO-responsive triggers rely on reaction with a nucleophilic amine or aniline,[22] indicating that an absorbance-tuning strategy would be better applied to an aniline-based rather than a phenol-based aza-BODIPY. While uncapping of an *o*-dichlorophenol produces a reliable 70-90 nm absorbance shift, the shift of aniline-based probes can vary significantly depending on other substituents and the capping group. Thus, chemical tuning was an essential step to design a probe with a substantial wavelength shift.

To this end, a panel of aza-BODIPY-based probes containing various NO-responsive moieties was synthesized (Figure 3a).[23] Acoustogenic Probe for Nitric Oxide (APNO) 1 featured an *o*-phenylenediamine group that reacts with NO to form a trizole.[24] While this probe did undergo a blue absorbance shift upon reaction with NO, ratiometric PA turn-on of 7.4-fold left room for improvement. This encouraged development of APNO-2 and APNO-3, which rely on the reaction of an *o*-aminophenol with NO to produce a diazonium intermediate that undergoes subsequent deamination.[25] Although this design improved the wavelength shift and dynamic range, slow reaction kinetics limited its utility. The development of APNO-4 revealed that the ideal NO-sensing moiety was an *o*-methoxy methylaniline, which is rapidly nitrosylated by NO.[26] Alkylation of the aniline prevented the slow kinetics of deamination, and the electron-withdrawing *N*-nitroso produced an 86 nm wavelength shift relative to the starting probe. This enabled ratiometric detection of probe activation using 770 and 680 nm light. Our final design, APNO-5, included a tetraalkylammonium PEG moiety that improved the solubility and tissue uptake of the probe.

In vitro characterization of APNO-5 revealed a 91 nm blue absorbance shift and corresponding 18.6-fold ratiometric turn-on upon reaction with NO (Figure 3b–d). The trigger proved highly selective for NO and was unresponsive to other reactive nitrogen, oxygen and carbonyl species. Additionally, APNO-5 was cell permeable and minimally toxic to RAW 264.7 macrophages, indicating its suitability for *in vivo* studies.

To evaluate APNO-5 *in vivo*, we employed a murine model of inflammation in which mice were subcutaneously administered with lipopolysaccharide (LPS) to induce NO production. Following treatment with LPS or saline, APNO-5 was subcutaneously administered, and ratiometric PAI was performed using 680 and 770 nm. PA images revealed that the 680/770 nm intensity ratio was initially similar for LPS and saline-treated animals; however, a 1.3-

fold increase in the signal ratio was consistently observed in LPS-treated mice 2 hours after probe administration (Figure 3e–f).

Development of APNO-5 enabled comparison of several probe designs aimed at sensing the same target. We found that the greatest wavelength shift upon activation produces the greatest ratiometric fold turn-on and dynamic range. This feature is especially important for *in vivo* imaging due to the background signal produced by endogenous absorbers. The APNO series also demonstrated the importance of probe solubility, as this can affect both the PA signal and the tissue uptake of the probe. Aggregation and consequent absorbance broadening can diminish the dynamic range of ratiometric fold-turn on and limit applicability for biological studies. In particular, ortho substitution of strongly electron-donating substituents resulted in diminished solubility of the APNO probes, and therefore the tetraalkylammonium PEG moiety was essential. This solubilizing group also played a key role in enabling tissue uptake following subcutaneous injection. When compared to other probes in the series, only APNO-5 resulted in clear diffusion of the PA signal into the surrounding tissue rather than pooling at the injection site. The addition of this group may prove to be a generalizable strategy for facilitating tissue uptake of lipophilic probes following subcutaneous administration.

During probe evaluation, we found that the *N*-nitroso product can undergo light-mediated reversion back to APNO-5 via denitrosylation after extended irradiation. While it did not impact our studies owing to the mild irradiation used, this result inspired us to explore the idea of small molecules capable of releasing species such as NO *in vivo* and providing a PA readout of the release. Modulation of NO levels in biological systems can provide insights into its many roles, and the use of a NIR photolabile PA donor would enable release and monitoring with high spatiotemporal control. This led to development of photocontrolled NO Donor (photoNOD) 1 and 2 (a water-soluble congener).[27] The photoNODs consist of an aza-BODIPY dye containing a photolabile *N*-nitroso (Figure 4a). NIR irradiation induces release of NO and the corresponding aniline, a process that is observable by ratiometric PAI (Figure 4c). While APNO-5 was designed with an *o*-methoxy group to increase aniline nucleophilicity, this feature was removed from the photoNODs to prevent re-capture of NO after release.

NO release from photoNOD-1 and 2 was demonstrated *in vitro* via irradiation in tissue-mimicking phantoms, and the identity of released NO was confirmed using EPR spectroscopy (Figure 4d–e). NO release was also observed *in vivo* following subcutaneous administration and irradiation (Figure 4f). The *N*-nitroso bond of both compounds was stable in the presence of numerous metal ions and reductants and was not susceptible to oxidation by cytochrome P450 enzymes (CYP450s). This indicated that these compounds do not form DNA-alkylating species known to result from metabolism of some *N*-nitroso-containing compounds.[28] To demonstrate the utility of our donor for *in vivo* NO release, we employed a murine tumor model. Tumors were implanted on both flanks of mice, and mice were treated with a systemic injection of photoNOD-1. NO was selectively released in one of the two tumors using NIR irradiation, and attenuation of tumor growth was observed in irradiated tumors compared to the control (Figure 4g).

The photoNODs represent a new class of PA probes designed for imaging analyte release with high spatiotemporal control following systemic administration. Like APNO, photoNOD was modified with a tetraalkylammonium PEG moiety to afford solubility and improve biological utility. While this was useful for subcutaneous administration, further studies indicated that the charged molecule likely undergoes rapid clearance following systemic administration.[29] Therefore, photoNOD-1 proved to be superior for tumor uptake. Further modifications to this structure with targeting functionalities may facilitate tissue-specific uptake and NO release, and this class of molecule may be expanded to enable release of a variety of biological species *in vivo*.

HYPOXIA-RESPONSIVE PROBES

Hypoxia refers to low tissue oxygenation and is known to lead to many changes in oxygen-dependent processes.[30] Chronic hypoxia occurs when the distance from blood supply to a tissue area is greater than oxygen's diffusion limit, while acute hypoxia occurs when arterial occlusions prevent blood delivery entirely. Hypoxia is known to be a pathological hallmark of solid tumors due to their irregular vasculature and rapid growth. Tumor hypoxia is associated with malignant phenotypes and treatment resistance; therefore, hypoxia detection is of significant clinical interest.[31] We hypothesized that a small-molecule hypoxia-responsive PA probe could provide an alternative to other detection methods that suffer from invasiveness and low resolution.

Although aryl nitro moieties are the most commonly employed hypoxia-responsive triggers for imaging probe development, we sought to establish a new trigger that overcomes several key drawbacks. Aryl nitro triggers can undergo reversible, one-electron reduction by CYP450 enzymes with nitroreductase activity.[32] Under hypoxic conditions, this species is further reduced to a highly reactive nitroso capable of crosslinking intracellular nucleophiles. While this process is typically hypoxia-selective, the reduction of aryl nitro triggers can also be mediated by certain nitroreductases in an oxygen-independent manner. Furthermore, activation of aryl nitro probes are associated with chronic rather than acute hypoxia detection.[32]

Our design instead drew inspiration from AQ4N, a hypoxia-responsive prodrug containing two *N*-oxide groups that undergo selective bioreduction by various CYP450 enzymes to unmask its cytotoxic DNA-binding properties.[33] This process is inhibited by oxygen binding to the heme iron, affording hypoxia selectivity. Unlike enzymatic aryl nitro reduction, *N*-oxide reduction is an irreversible process .[34,35] With this in mind, we designed Hypoxia Probe 1 (HyP-1), which consists of an aza-BODIPY dye containing an aniline *N*-oxide (Figure 5a).[36]

Photophysical characterization of HyP-1 and the corresponding aniline (red-HyP-1) revealed that *N*-oxide reduction produces a significant red absorbance shift (Figure 5d). PA images in a tissue-mimicking phantom show that HyP-1 produces no signal at 770 nm, while red-HyP-1 produces a strong, concentration dependent signal (Figure 5b–c). Hypoxia detection can therefore be carried out by detecting a 770 nm signal enhancement (ΔPA). Additionally, HyP-1 and red-HyP-1 are fluorescent and can be used for ratiometric fluorescence imaging

of hypoxia. This enabled *in vitro* and cellular studies using fluorescence imaging and confirmation of *in vivo* imaging results with a second imaging modality.

To verify that hypoxia-selective response of the *N*-oxide trigger, *in vitro* studies were performed in which HyP-1 was incubated with NADPH-supplemented rat liver microsomes (RLMs) in hypoxia and normoxia. The hypoxic condition selectively resulted in a 105-fold ratiometric fluorescent turn-on. To elucidate the mechanism of this response, experiments were performed in which RLMs were treated with an Fe(II) chelator. The lack of inhibition under these conditions indicated that HyP-1 was not being reduced from labile iron released from the microsomes. However, turnover was inhibited by both the exclusion of NADPH and the addition of a CYP450 reductase inhibitor, diphenyl iodonium chloride, suggesting that reduction is CYP450-mediated. Finally, heat inactivation of the microsomes did not inhibit turnover, providing evidence that HyP-1 can undergo both enzymatic and non-enzymatic heme-mediated reduction under hypoxic conditions.[34] These results were confirmed in cell culture (Figure 5f–g).

To demonstrate *in vivo* imaging with HyP-1, we first employed a murine 4T1 tumor model (Figure 5h–k). Tumors were grown to 300-400 mm^3, at which point HyP-1 was administered via tail vein injection and PAI was performed at various time points. Images were compared to those acquired before probe administration, and a consistent signal enhancement (ΔPA) was observed in the tumors, while no signal change occurred in the control flank. Interestingly, the high resolution of the PA images revealed subtumoral regions where signal accumulation was greatest, which we hypothesized to indicate areas of most significant hypoxia.

Since the *N*-oxide trigger was designed to respond to both types of hypoxia, it was important demonstrate the activation of HyP-1 in an acute hypoxia model. To this end, we employed a murine hindlimb ischemia model in which surgical ligation of the femoral artery produces an ischemic limb. Following surgical ligation, HyP-1 was administered into both limbs and PAI revealed that activation occurred only in the ischemic limb. This experiment demonstrates an important contrast between HyP-1 and aryl nitro-based probes, which require enzyme upregulation. In contrast, HyP-1 can respond to hypoxia before significant changes in gene expression occur and is therefore applicable for acute hypoxia detection.[37]

HyP-1 was the first example of an acoustogenic probe used *in vivo*. This work enabled determination of essential characteristics for PA probes; including a large wavelength shift, high extinction coefficient, and rapid response. Compatibility with fluorescence imaging was advantageous in this study because it enabled multimodal imaging and facile *in vitro* evaluation. A direct comparison between fluorescence and PAI in this study revealed the far superior resolution of PAI in deep tissue. Finally, a key component of HyP-1 development was the hypoxia-responsive *N*-oxide trigger, which may prove to be a versatile mechanism for hypoxia detection.

One challenge of using HyP-1 for PAI is that hypoxia detection relies on a signal enhancement at a single wavelength. As mentioned previously, PA signal is subject to fluctuations in laser source intensity, tissue properties, and local probe concentration.

Ratiometric imaging can account for these factors; however, the low extinction coefficient of HyP-1 and limited imaging range (680-950 nm) of commercial PA tomographers prevented ratiometric imaging with this probe. We sought to improve this design by shifting the wavelength of both HyP-1 and red-HyP-1 further into the PAI window such that both would be detectable using PAI. It is well-established that increasing electron donation into the aza-BODIPY platform provides a red shift in the absorbance profile, and in fact this is the basis of many of our PA probe designs.[16] Thus, we designed ratiometric Hypoxia Probe 1 (rHyP-1) with an electron-donating dialkyl amine in place of the methoxy group of HyP-1.[38] To further tune photophysical properties and CYP450-mediated activation, a small panel of ratiometric hypoxia probes was synthesized containing various dialkyl anilines including diethyl, dimethyl, dipropyl, piperidine and morpholine analogs (Figure 5a). Photophysical characterization revealed that these probes were indeed red-shifted relative to HyP-1, with absorbance maxima for the *N*-oxides and turned over products ranging from 718-749 nm and 758-818 nm, respectively (Figure 5b–c).

This new series was evaluated *in vitro* using RLMs in both hypoxic and normoxic conditions (Figure 6c). The aniline substituents influenced probe solubility, reactivity with RLMs, and the wavelength shift between *N*-oxide and aniline. Based on collected data, rHyP-1 was determined to be optimal for *in vivo* applications. To evaluate this probe *in vivo*, we again relied on a 4T1 murine tumor model. rHyP-1 was locally administered into both tumor-bearing and control flanks of mice, and PAI at 820 and 750 nm was performed at various time points following injection. The 820/720 nm signal ratio remained unchanged in the control flank but steadily increased in the tumor, reaching an average 1.2-fold ratiometric turn-on after one hour (Figure 6f). 3D rendering of tumor images enabled visualization of "hot spots" within the tumor where ratiometric signal was greatest relative to the rest of the tumor (Figure 6e). These regions were hypothesized to correspond to subtumoral volumes where hypoxia is greatest. Ratiometric signal within specific tumor regions could be evaluated by demonstrating that the PA ratio increases with tumor depth in 2 mm imaging sections (Figure 5d).

Overall, rHyP-1 demonstrated that photophysical tuning can improve the PA properties of acoustogenic probes. HyP-1 and rHyP-1 both offer certain advantages and are complementary in their applicability. For instance, while rHyP-1 is superior for ratiometric PAI, HyP-1 is more useful for multimodal imaging. With respect to rHyP-1, the ability to discern specific subtumoral hypoxic regions is of critical importance as the extent of hypoxia can be used to guide radiotherapy and predict prognosis.[39]

CONCLUSION

Over the past decade, PAI has approached the forefront of preclinical imaging modalities. To date, PAI has been used clinically for label-free imaging of breast cancer,[40] thyroid cancer,[41] and inflammatory arthritis.[42] The safe irradiation, high resolution, clinically-relevant depths, and affordability make it an attractive tool for various biomedical applications. There is currently significant interest in expanding the applications of PAI through the use of responsive probes. To date, we have demonstrated how chemical reactivity and photophysical tuning can be employed to rationally design small-molecule PA probes, and

our efforts have produced probes for Cu(II), NO, and hypoxia. More importantly, the design principles employed in these studies are generalizable and can be employed for the development of acoustogenic probes responding to a variety of targets.

The wavelength tunbability of the aza-BODIPY platform via chemical modification makes it an attractive PA chromophore and inspired its use in our acoustogenic probe designs. However, other NIR dye platforms such as cyanine and semicyanine have also found applications in the development of activatable PA probes.[11] The choice of PA chromophore for a particular application relies on characteristics such as photostability, biocompatibility, and ability to respond to a given analyte to provide a change in PA output. Additionally, while our work focuses on small-molecule-based probes, many nanomaterial and polymer-based activatable PA probes have also been developed.[11,43,44] These different probe types can offer complementary advantages depending on the desired applications.

Our future work will be aimed at continuing to explore new designs for small-molecule PA probes and applying developed probes for *in vivo* studies. For example, monitoring reactive species throughout tumor progression will help elucidate specific roles. The non-invasiveness of PAI makes it an attractive approach for these studies since longitudinal tracking of animals can be performed without sacrificing and *ex vivo* analysis. Furthermore, the high resolution of PAI enables imaging of smaller microenvironments within one tumor. Simultaneous imaging of endogenous chromophores such as hemoglobin enables visualization of these subtumoral regions in the context of vasculature, a feature that is unique to this imaging modality. Overall, the combination of this powerful technique with acoustogenic probes is poised to enable real-time analysis of complex tissue microenvironments with high resolution in a non-invasive manner.

ACKNOWLEDGMENT

HJK was supported by the Tissue Microenvironment Training Grant (T32 EB019944) and a Beckman Graduate Fellowship. Additional funding came from the Alfred P. Sloan fellowship (FG-2017-8964 to JC) and the National Science Foundation (CHE 1752879 to JC).

BIOGRAPHICAL INFORMATION

Hailey Knox received her B.S. in chemistry from the University of Idaho in 2015. She is currently a Beckman Graduate Fellow and Tissue Microenvironment Program Trainee at the University of Illinois of Urbana Champaign where she works in the lab of Prof. Jefferson Chan.

Jefferson Chan received his Ph.D. in 2011, with Prof. Andrew Bennet at Simon Fraser University. From 2011 to 2014, he was a Human Frontiers Science Program postdoctoral fellow with Prof. Christopher Chang at the University of California, Berkeley. In 2014, he began his independent career at the University of Illinois at Urbana-Champaign where he is currently an Assistant Professor of Chemistry. His group focuses on developing stimuli-responsive probes for various imaging modalities including photoacoustic tomography.

REFERENCES

(1). James ML; Gambhir SS A Molecular Imaging Primer: Modalities, Imaging Agents, and Applications. Physiol. Rev 2012, 92, 897–965. [PubMed: 22535898]

(2). Chan J; Dodani SC; Chang CJ Reaction-Based Small-Molecule Fluorescent Probes for Chemoselective Bioimaging. Nat. Chem 2012, 4, 973–984. [PubMed: 23174976]

(3). Grimm JB; Heckman LM; Lavis LD The Chemistry of Small-Molecule Fluorogenic Probes. Prog. Mol. Biol. Transl. Sci 2013, 113, 1–34. [PubMed: 23244787]

(4). Ntziachristos V Going Deeper than Microscopy: The Optical Imaging Frontier in Biology. Nat. Methods 2010, 7, 603–614. [PubMed: 20676081]

(5). Wang LV; Yao J. A Practical Guide to Photoacoustic Tomography in the Life Sciences. Nat. Methods 2016, 13, 627–638. [PubMed: 27467726]

(6). Choi W; Park EY; Jeon S; Kim C Clinical Photoacoustic Imaging Platforms. Biomed. Eng. Lett 2018, 8, 139–155. [PubMed: 30603199]

(7). Borg RE; Rochford J Molecular Photoacoustic Contrast Agents (MPACs): Design Principles & Applications. Photochem. Photobiol 2018, 0–3.

(8). Abuteen A; Zanganeh S; Akhigbe J; Samankumara LP; Aguirre A; Biswal N; Braune M; Vollertsen A; Röder B; Brückner C; Zhu Q The Evaluation of NIR-Absorbing Porphyrin Derivatives as Contrast Agents in Photoacoustic Imaging. Phys. Chem. Chem. Phys. PCCP 2013, 15, 18502–18509. [PubMed: 24071709]

(9). Sano K; Ohashi M; Kanazaki K; Makino A; Ding N; Deguchi J; Kanada Y; Ono M; Saji H Indocyanine Green-Labeled Polysarcosine for in Vivo Photoacoustic Tumor Imaging. Bioconjug. Chem 2017, 28, 1024–1030. [PubMed: 28166625]

(10). Levi J; Kothapalli SR; Ma T; Hartman K; Khuri-Yakub BT; Gambhir SS Design, Synthesis, and Imaging of an Activatable Photoacoustic Probe. J. Am. Chem. Soc 2010, 132, 11264–11269. [PubMed: 20698693]

(11). Reinhardt CJ; Chan J Development of Photoacoustic Probes for in Vivo Molecular Imaging. Biochemistry 2018, 57, 194–199. [PubMed: 29022344]

(12). Levi J; Kothapalli SR; Ma T; Hartman K; Khuri-yakub BT; Sam S Design and Synthesis of an Activatable Photoacoustic Probe. J. Am. Chem. Soc 2010, No. 132, 11264–11269. [PubMed: 20698693]

(13). Frenette M; Hatamimoslehabadi M; Bellinger-Buckley S; Laoui S; La J; Bag S; Mallidi S; Hasan T; Bouma B; Yelleswarapu C; Rochford J Shining Light on the Dark Side of Imaging: Excited State Absorption Enhancement of a Bis-Styryl BODIPY Photoacoustic Contrast Agent. J. Am. Chem. Soc 2014, 136, 15853–15856. [PubMed: 25329769]

(14). Zhuang Y; Xu Q; Huang F; Gao P; Zhao Z; Lou X; Xia F Ratiometric Fluorescent Bioprobe for Highly Reproducible Detection of Telomerase in Bloody Urines of Bladder Cancer Patients. ACS Sensors 2016, 1, 572–578.

(15). Jokic T; Borisov SM; Saf R; Nielsen D. a.; Kühl M; Klimant I Highly Photostable Near-Infrared Fluorescent PH Indicators and Sensors Based on BF2-Chelated Tetraarylazadipyrromethene Dyes. Anal. Chem 2012, 84, 6723–6730. [PubMed: 22738322]

(16). Jiang X-D; Li S; Guan J; Fang T; Liu X; Xiao L-J Recent Advances of the Near-Infrared Fluorescent Aza-BODIPY Dyes. Curr. Org. Chem 2016, 20, 1736–1744.

(17). Li H; Zhang P; Smaga LP; Hoffman RA; Chan J Photoacoustic Probes for Ratiometric Imaging of Copper(II). J. Am. Chem. Soc 2015, 137, 15628–15631. [PubMed: 26652006]

(18). Giampietro R; Spinelli F; Contino M; Colabufo NA The Pivotal Role of Copper in Neurodegeneration: A New Strategy for the Therapy of Neurodegenerative Disorders. Mol. Pharm 2018, 15, 808–820. [PubMed: 29323501]

(19). Roberts S; Seeger M; Jiang Y; Mishra A; Sigmund F; Stelzl A; Lauri A; Symvoulidis P; Rolbieski H; Preller M; Deán-Ben XL; Razansky D; Orschmann T; Desbordes SC; Vetschera P; Bach T; Ntziachristos V; Westmeyer GG Calcium Sensor for Photoacoustic Imaging. J. Am. Chem. Soc 2018, 140, 2718–2721. [PubMed: 28945084]

(20). Hunter RA; Storm WL; Coneski PN; Schoenfisch MH Inaccuracies of Nitric Oxide Measurement Methods in Biological Media. Anal. Chem 2013, 85, 1957–1963. [PubMed: 23286383]

(21). Sharma R; Seo J-W; Kwon S In Vivo Imaging of Nitric Oxide by Magnetic Resonance Imaging Techniques. J. Nanomater 2014, 2014, 1–13.

(22). Hilderbrand SA; Lim MH; Lippard SJ Fluorescence-Based Nitric Oxide Detection. Top. Fluoresc. Spectrosc 2005, 9, 163–188.

(23). Reinhardt CJ; Zhou EY; Jorgensen MD; Partipilo G; Chan J A Ratiometric Acoustogenic Probe for in Vivo Imaging of Endogenous Nitric Oxide. J. Am. Chem. Soc 2018, 140, 1011–1018. [PubMed: 29313677]

(24). Kojima H; Nakatsubo N; Kikuchi K; Kawahara S; Kirino Y; Nagoshi H; Hirata Y; Nagano T Detection and Imaging of Nitric Oxide with Novel Fluorescent Indicators: Diaminofluoresceins. Anal. Chem 1998, 70, 2446–2453. [PubMed: 9666719]

(25). Shiue T-W; Chen Y-H; Wu C-M; Singh G; Chen H-Y; Hung C-H; Liaw W-F; Wang Y-M Nitric Oxide Turn-on Fluorescent Probe Based on Deamination of Aromatic Primary Monoamines. Inorg. Chem 2012, 51, 5400–5408. [PubMed: 22486484]

(26). Mao Z; Jiang H; Li Z; Zhong C; Zhang W; Liu Z An N-Nitrosation Reactivity-Based Two-Photon Fluorescent Probe for the Specific in Situ Detection of Nitric Oxide. Chem. Sci 2017, 8, 4533–4538. [PubMed: 28660066]

(27). Zhou EY; Knox HJ; Reinhardt CJ; Partipilo G; Nilges MJ; Chan J Near-Infrared Photoactivatable Nitric Oxide Donors with Integrated Photoacoustic Monitoring. J. Am. Chem. Soc 2018, 140, 11686–11697. [PubMed: 30198716]

(28). Tricker AR; Preussmann R Carcinogenic N-Nitrosamines in the Diet: Occurrence, Formation, Mechanisms and Carcinogenic Potential. Mutat. Res. Toxicol 1991, 259, 277–289.

(29). Berezin MY; Guo K; Akers W; Livingston J; Solomon M; Lee H; Liang K; Agee A; Achilefu S Rational Approach To Select Small Peptide Molecular Probes Labeled with Fluorescent Cyanine Dyes for in Vivo Optical Imaging. Biochemistry 2011, 50, 2691–2700. [PubMed: 21329363]

(30). Semenza GL Hypoxia-Inducible Factors in Physiology and Medicine. Cell 2012, 148, 399–408. [PubMed: 22304911]

(31). Walsh JC; Lebedev A; Aten E; Madsen K; Marciano L; Kolb HC The Clinical Importance of Assessing Tumor Hypoxia : Relationship of Tumor Hypoxia to Prognosis. Antioxidants Redox Signal. 2014, 21, 1516–1554.

(32). Kizaka-Kondoh S; Konse-Nagasawa H Significance of Nitroimidazole Compounds and Hypoxia-Inducible Factor-1 for Imaging Tumor Hypoxia. Cancer Sci. 2009, 100, 1366–1373. [PubMed: 19459851]

(33). Patterson LH; McKeown SR AQ4N: A New Approach to Hypoxia-Activated Cancer Chemotherapy. Br. J. Cancer 2000, 83, 1589–1593. [PubMed: 11104551]

(34). Takekawa K; Sugihara K; Kitamura S; Ohta S Enzymatic and Non-Enzymatic Reduction of Brucine N -Oxide by Aldehyde Oxidase and Catalase. Xenobiotica 2001, 31, 769–782. [PubMed: 11765140]

(35). Sugiura M; Iwasaki K; Kato R Reduction of Tertiary Amine N-Oxides by Liver Microsomal Cytochrome P-450. Mol. Pharmacol 1976, 12, 322–334. [PubMed: 4725]

(36). Knox HJ; Hedhli J; Kim TW; Khalili K; Dobrucki LW; Chan J A Bioreducible N-Oxide-Based Probe for Photoacoustic Imaging of Hypoxia. Nat. Commun 2017, 8, 1794. [PubMed: 29176550]

(37). Lee CW; Stabile E; Kinnaird T; Shou M; Devaney JM; Epstein SE; Burnett MS Temporal Patterns of Gene Expression after Acute Hindlimb Ischemia in Mice: Insights into the Genomic Program for Collateral Vessel Development. J. Am. Coll. Cardiol 2004, 43, 474–482. [PubMed: 15013133]

(38). Knox HJ; Kim TW; Zhu Z; Chan J Photophysical Tuning of N -Oxide-Based Probes Enables Ratiometric Photoacoustic Imaging of Tumor Hypoxia. ACS Chem. Biol 2018, acschembio.8b00099.

(39). Horsman MR; Mortensen LS; Petersen JB; Busk M; Overgaard J Imaging Hypoxia to Improve Radiotherapy Outcome. Nat. Rev. Clin. Oncol 2012, 9, 674–687. [PubMed: 23149893]

(40). Heijblom M; Piras D; Brinkhuis M; van Hespen JCG; van den Engh FM; van der Schaaf M; Klaase JM; van Leeuwen TG; Steenbergen W; Manohar S; Jemal A; Siegel R; Naishadham D; Jemal A; Berry DA; Berg WA; Mousa D. S. Al; Ryan EA; Mello-Thoms C; et al. Photoacoustic

Image Patterns of Breast Carcinoma and Comparisons with Magnetic Resonance Imaging and Vascular Stained Histopathology. Sci. Rep 2015, 5, 11778. [PubMed: 26159440]

(41). Yang M; Zhao L; He X; Su N; Zhao C; Tang H; Hong T; Li W; Yang F; Lin L; Zhang B; Zhang R; Jiang Y; Li C Photoacoustic/Ultrasound Dual Imaging of Human Thyroid Cancers: An Initial Clinical Study. Biomed. Opt. Express 2017, 8, 3449–3457. [PubMed: 28717580]

(42). Jo J; Xu G; Cao M; Marquardt A; Francis S; Gandikota G; Wang X A Functional Study of Human Inflammatory Arthritis Using Photoacoustic Imaging. Sci. Rep 2017, 7, 15026. [PubMed: 29101339]

(43). Miao Q; Pu K Emerging Designs of Activatable Photoacoustic Probes for Molecular Imaging. Bioconjug. Chem 2016, 27, 2808–2823. [PubMed: 27998078]

(44). Zeng L; Ma G; Lin J; Huang P Photoacoustic Probes for Molecular Detection: Recent Advances and Perspectives. Small 2018, 1800782.

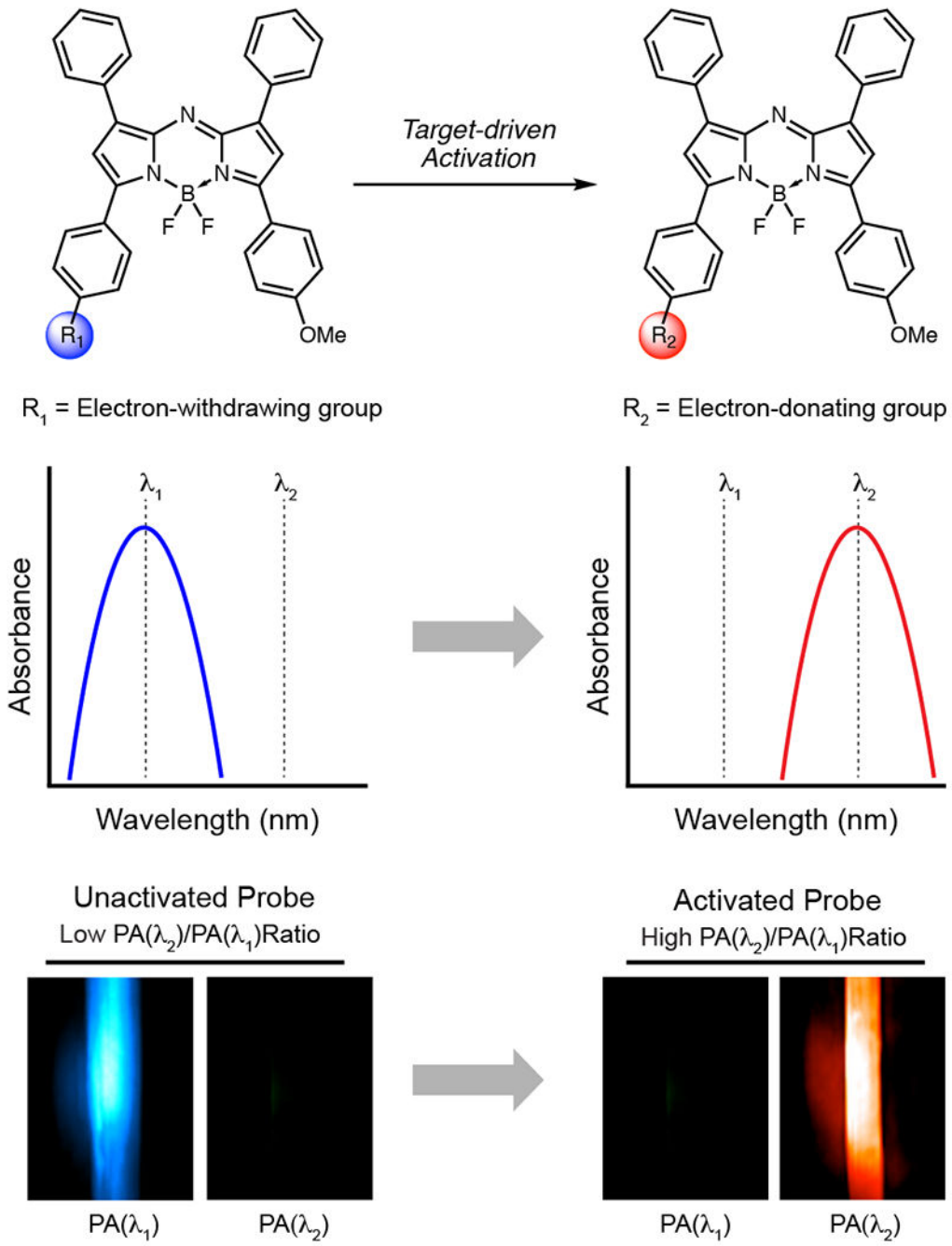

Figure 1.

Schematic illustration of ratiometric imaging with acoustogenic probes. Probe activation results in a spectral change, and PAI is performed at wavelengths corresponding to both the unactivated and activated probe forms. A high ratiometric PA signal corresponds to a large proportion of activated probe, indicating target detection.

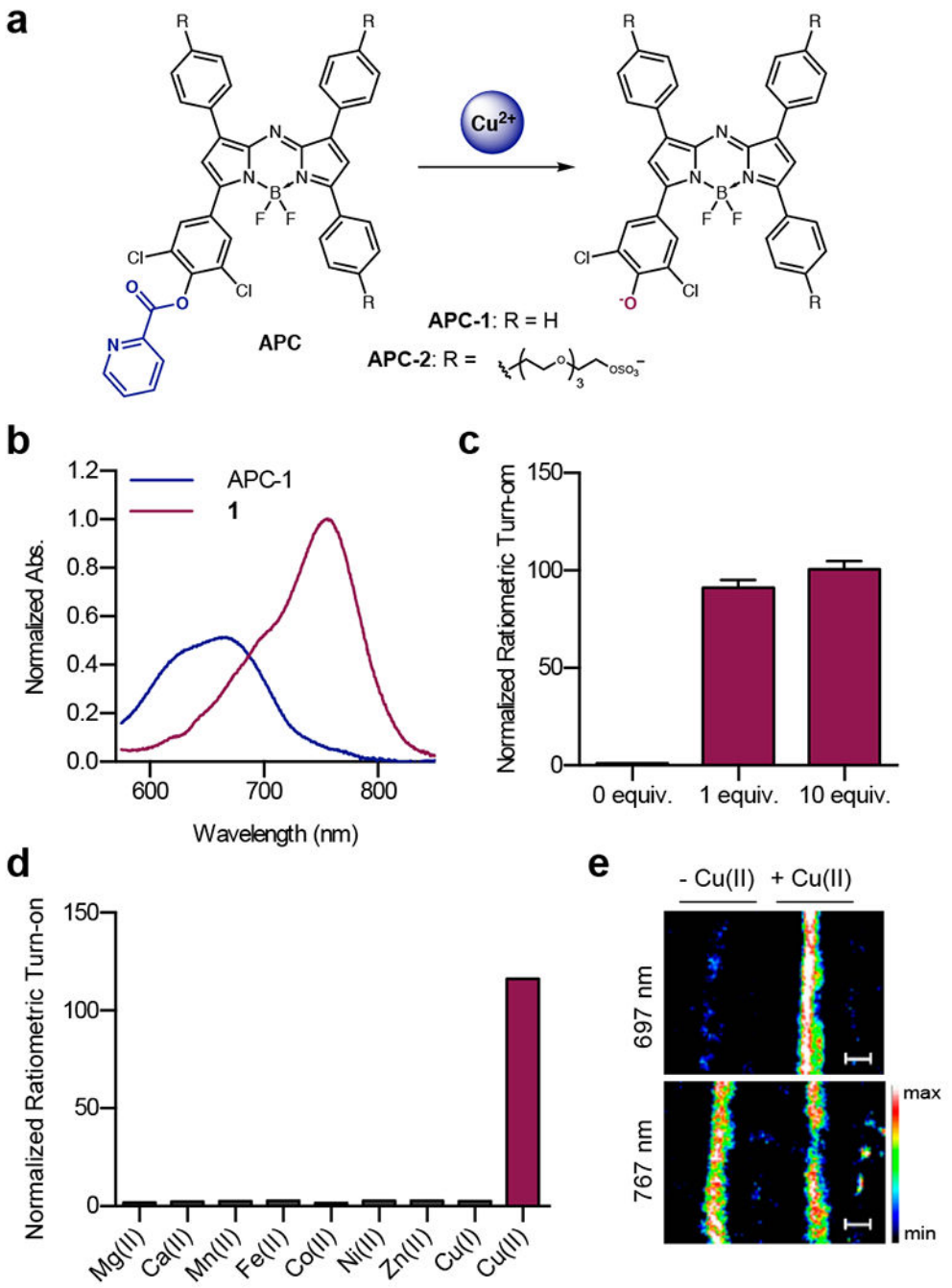

Figure 2.

a) Chemical structure of APC probes and the products formed after Cu(II) treatment. b) Normalized absorbance of APC-1 and its hydrolyzed product (1). c) Normalized ratiometric PA fold turn-on of APC-2 upon treatment with Cu(II). d) Normalized ratiometric PA fold turn-on of APC-2 upon treatment with various metal ions. e) PA images of solutions of APC-2 in fluorinated ethylene propylene (FEP) tubes in a tissue-mimicking phantom with or without the addition of Cu(II).

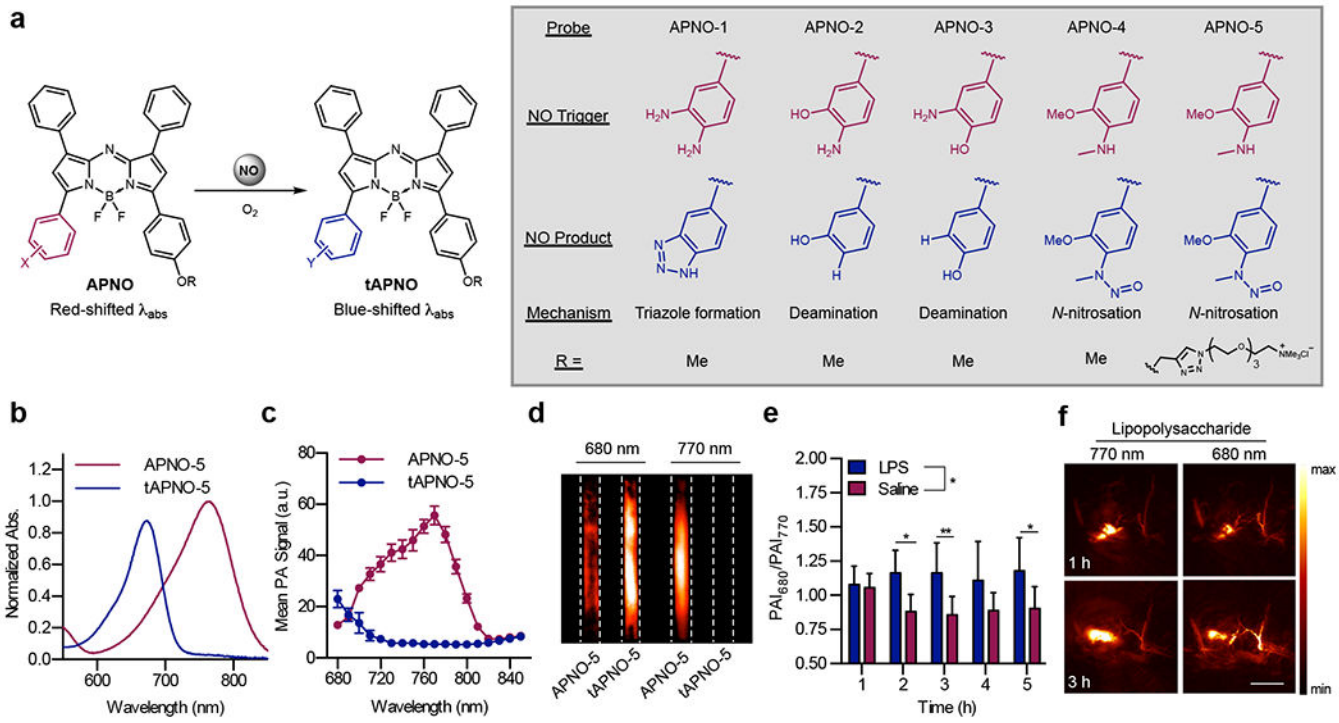

Figure 3.

a) Chemical structures and sensing mechanisms of the APNO and tAPNO series. b) Normalized absorbance spectra and c) PA spectra of APNO-5 and tAPNO-5. d) PA images of APNO-5 and tAPNO-5. e) Ratiometric PA signal and f) representative images of APNO-5 in a murine model of inflammation.

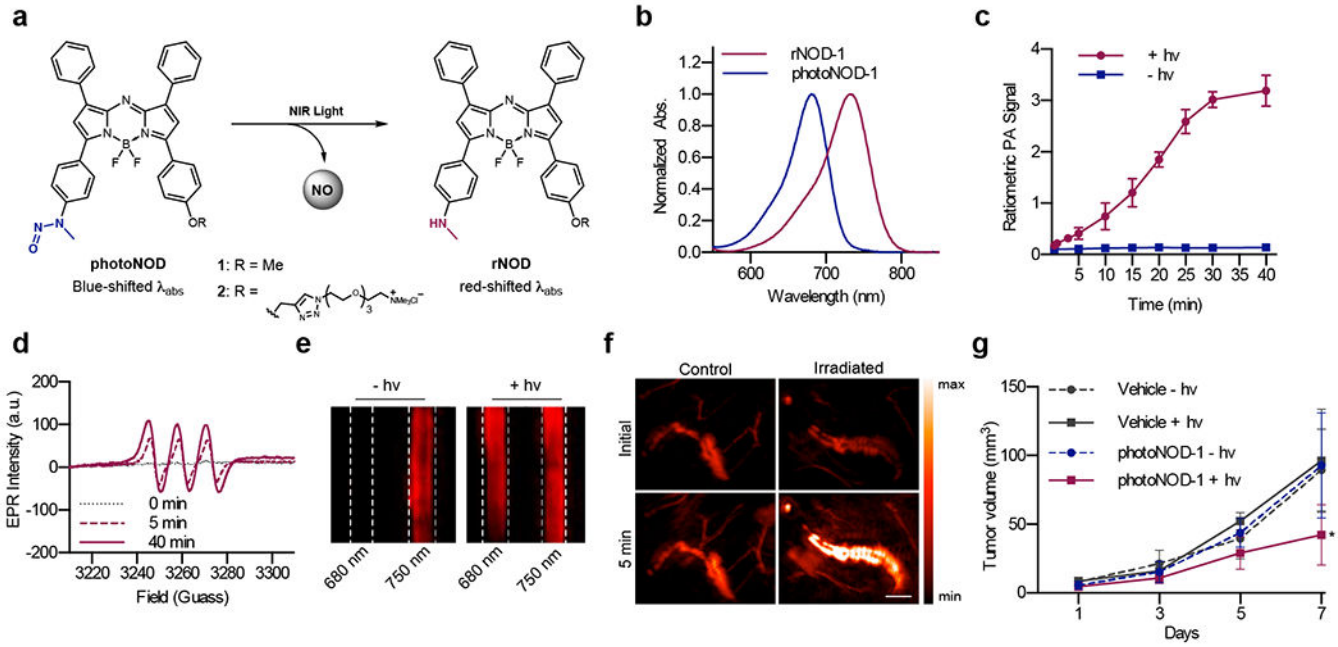

Figure 4.

a) Chemical structure of photoNODs and rNODs. b) Normalized absorbance spectra of photoNOD-1 and rNOD-1 in $CHCl_3$. c) Time-dependent ratiometric PA signal of photoNOD-1 produced with or without irradiation. d) EPR spectra of photoNOD-1 collected after 0, 5 and 40 minutes of irradiation in the presence of $Fe(MGD)_2$. e) PA images of photoNOD-2 with or without 5 min of irradiation. f) PA images of photoNOD-2 after subcutaneous injection and a 5 min period with/without irradiation. g) Tumor volumes following repeated systemic administration of photoNOD-1 or vehicle with/without irradiation.

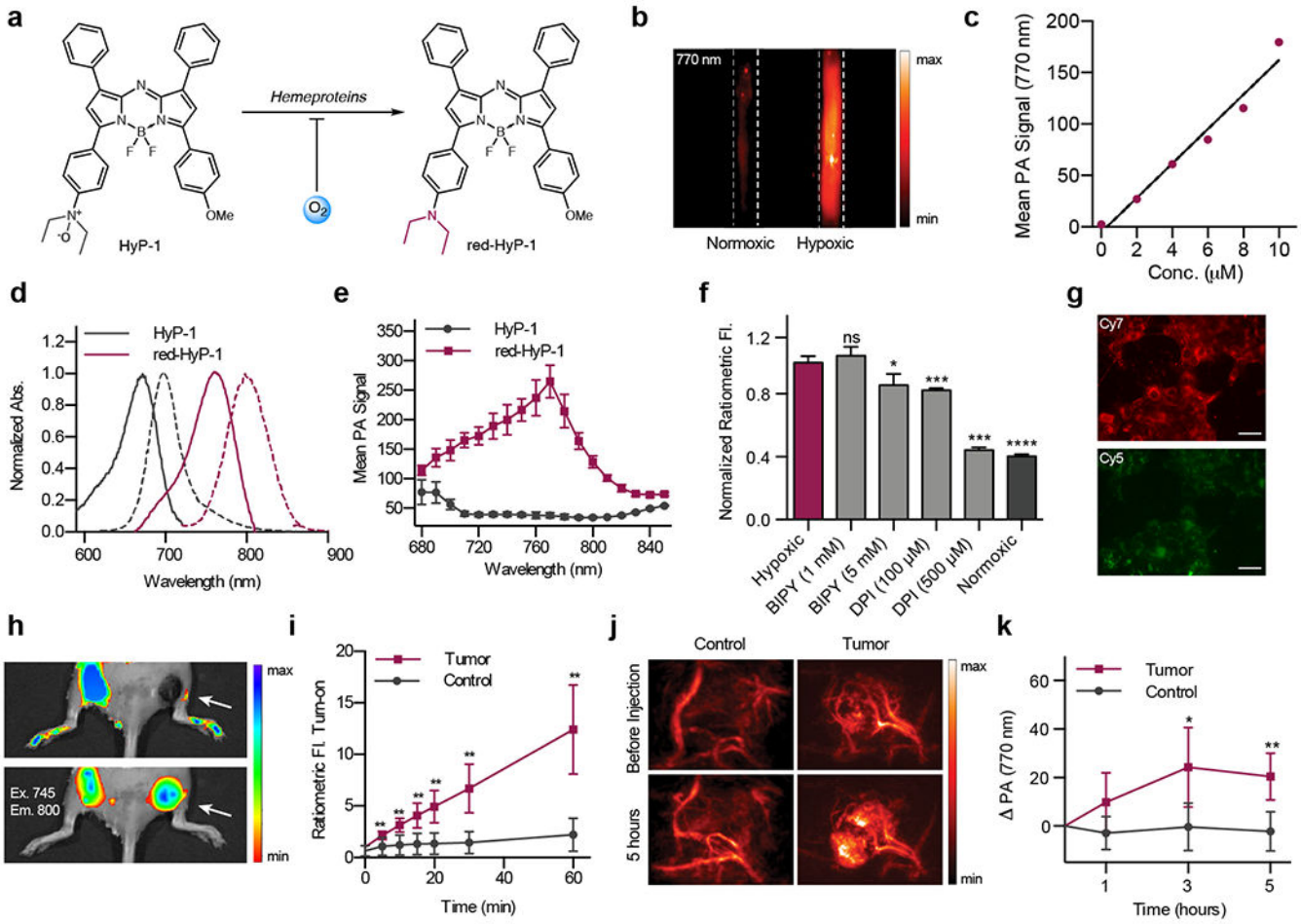

Figure 5.

a) Chemical structure of HyP-1 and red-HyP-1. b) PA image HyP-1 treated with RLMs under normoxic or hypoxic conditions. c) Concentration-dependent PA signal of red-HyP-1 in a tissue mimicking phantom. d) Normalized absorbance (solid) and emission (dashed) spectra of HyP-1 and red-HyP-1. e) PA spectra of HyP-1 and red-HyP-1. f) Normalized ratiometric fluorescence of 4T1 cells following treatment with HyP-1 in hypoxic (red, light grey) or normoxic (dark grey) conditions. g) 4T1 cells stained with HyP-1 and incubated under hypoxic conditions. Cy5 and Cy7 filters used for visualization of HyP-1 and red-HyP-1, respectively. h) Representative images and i) quantification of ratiometric fluorescence of HyP-1 following intratumoral and subcutaneous (control) injection. j) Representative images and k) quantification of PA signal of HyP-1 in a murine tumor model following systemic injection.

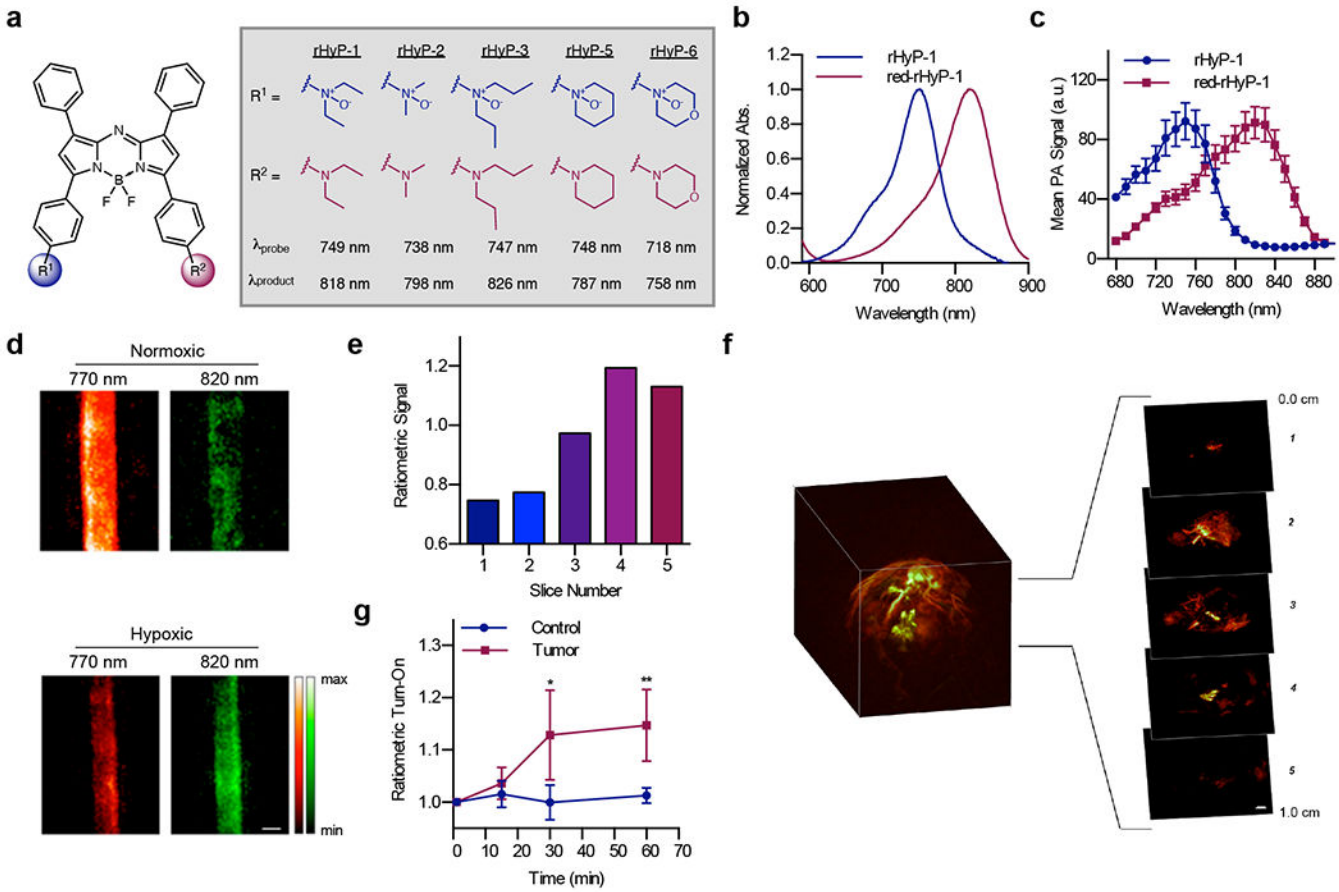

Figure 6.

a) Chemical structures of the rHyP series. b) Normalized absorbance and c) PA spectra of rHyP-1 and red-rHyP-1 in $CHCl_3$. d) PA images of rHyP-1 solutions treated with RLMs in normoxic and hypoxic conditions. e) Ratiometric PA signal in 2 mm slices of a PA reconstruction of a 4T1 tumor following administration of rHyP-1. f) Ratiometric PA fold turn-on of rHyP-1 in tumor-bearing and control flanks. g) Representative PA 3D reconstruction of a 4T1 tumor following administration of rHyP-1.